Photochemical Aging of Atmospheric Particulate Matter in the Aqueous Phase

Frank Leresche[1,2,*], Joseph R. Salazar[3], David J. Pfotenhauer[4], Michael P. Hannigan[4], Brian J. Majestic[3], Fernando L. Rosario-Ortiz[1,2]

[1]Department of Civil, Environmental and Architectural Engineering, University of Colorado at Boulder, Boulder, 80309, USA
[2]Environmental Engineering Program, University of Colorado Boulder, Colorado 80309, USA
[3]Department of Chemistry and Biochemistry, University of Denver, Denver, 80208, USA
[4]Department of Mechanical Engineering, University of Colorado at Boulder, Boulder, 80309, USA

**Correspondence to* Frank Leresche (Frank.Leresche@Colorado.edu)

Graphical Abstract

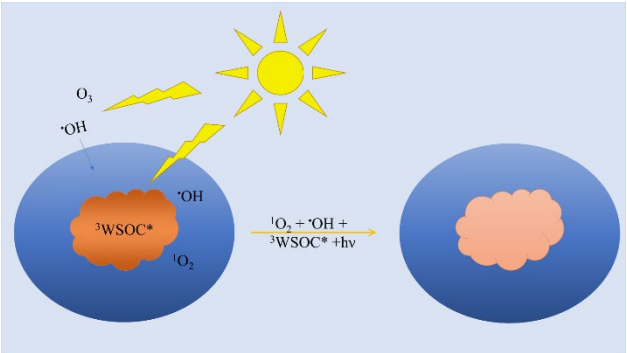

Abstract.

This study focused on the photoaging of atmospheric particulate matter smaller than 2.5 microns ($PM_{2.5}$) in the aqueous phase. $PM_{2.5}$ were collected during a winter, a spring and a summer campaign in urban and rural settings in Colorado and extracted into water. The aqueous extracts were photoirradiated using simulated sunlight, the production rate ($r_{\bullet OH}$) and the effects of hydroxyl radical ($^{\bullet}OH$) measured as well as the optical properties as a function of the photoaging of the extracts. $r_{\bullet OH}$ was seen to have a strong seasonality with low mean values for the winter and spring extracts (4.8 and 14 fM s^{-1} mg_C^{-1} L respectively) and a higher mean value for the summer extracts (65.4 fM s^{-1} mg_C^{-1} L).

For the winter extracts, $^{\bullet}OH$ was seen to mostly originate from nitrate photolysis while for the summer extracts a correlation was seen between $r_{\bullet OH}$ and iron concentration. The extent of photobleaching of the extracts correlated with $r_{\bullet OH}$, the correlation also indicated that non-$^{\bullet}OH$ processes took place. Using the $^{\bullet}OH$ measurements and singlet oxygen ($^1O_2$) measurements, the half-life of a selection of compounds was modeled in the atmospheric aqueous phase to be between 1.9 and 434 hours.

1 Introduction

Atmospheric particulate matter smaller than 2.5 µm ($PM_{2.5}$) is an important subject of research due to the uncertainties around its impact on radiative forcing and global warming as well as its detrimental effects on human health.[1-3] $PM_{2.5}$ include an inorganic fraction, mostly composed of sulfates, nitrates, ammonium, chloride and metals in low concentration, and an organic fraction.[4-6] The organic fraction of $PM_{2.5}$ is produced by a variety of processes that can be natural (e.g. emission from plants, wildfires, atmospheric oxidation of gas-phase species) but also anthropogenic (e.g. road traffic, burning processes). Once in the atmosphere, $PM_{2.5}$ soluble compounds can diffuse to the atmospheric aqueous phase forming water soluble organic carbon (WSOC) that can undergo further aging while in the aqueous phase.[7-9]. Additionally, less soluble $PM_{2.5}$ compounds can undergo gas phase oxidation reactions with ozone or hydroxyl radicals ($^{\bullet}OH$) that lead to more soluble products that can then be entrained into the atmospheric aqueous phase also forming WSOC.

The aqueous phase aging of WSOC includes photochemical reactions whose importance and effects on WSOC are not fully characterized. These photochemical reactions include direct phototransformation (equation 1, where WSOC' represents a transformed WSOC) and indirect reactions with reactive intermediates such as $^{\bullet}OH$ and potentially with excited triplet state of the WSOC (^{3}WSOC*) or singlet oxygen ($^1O_2$). In addition to these condensed phase processes, oxidants present in the gas phases such as $^{\bullet}OH$ can diffuse into the aqueous phase and react with WSOC. ^{3}WSOC* and $^1O_2$ are generated from WSOC irradiation (equations 2 and 3) while for $^{\bullet}OH$ the most important condensed phase sources of $^{\bullet}OH$ are believed to be nitrate photolysis (equation 4) and the Fenton or photo-Fenton reactions (equations. 5 and 6). Additionally, depending on the composition of the extract, other reactions such as nitrite or WSOC photolysis could also be important sources of $^{\bullet}OH$ (equations. 7 and 8).[10, 11] $^{\bullet}OH$ is probably one of the main species driving the indirect phototransformation of WSOC in the aqueous phase. Based on the relative steady-state concentration of $^1O_2$ and $^{\bullet}OH$, ($[^1O_2]_{ss}$ and $[^{\bullet}OH]_{ss}$ respectively) and second-order rate constants of compounds towards $^1O_2$ and $^{\bullet}OH$, it was shown that $^1O_2$ should play an important role in the phototransformation of some classes of aromatic compounds,[12] while for some phenols it was shown that ^{3}WSOC* should be the dominant oxidant.[13] Schemes presenting and discussing the aforementioned reactions are presented in the following articles.[14-16]

WSOC + hν	→ WSOC'	(1)	Del Vecchio & Blough[17]
WSOC + hν	→ ^{1}WSOC* → ^{3}WSOC*	(2)	McNeill & Canonica[15]
^{3}WSOC*+O_2	→ WSOC + $^1O_2$	(3)	McNeill & Canonica[15]
NO_3^- + hν + H^+	→ $^{\bullet}OH$ + NO_2	(4)	Vione et al.[14]
Fe^{2+} + H_2O_2	→ Fe^{3+} + $^{\bullet}OH$ + OH^-	(5)	White et al.[18]
Fe^{3+} +H_2O + hν	→ Fe^{2+} + $^{\bullet}OH$ + H^+	(6)	White et al.[18]
NO_2^- + hν + H^+	→ $^{\bullet}OH$ + NO	(7)	Vione et al.[14]

$$WSOC + h\nu \rightarrow WSOC' + {}^{\bullet}OH \quad (8)$$ White et al.[18]

The objective of this paper was to characterize the photoaging of $PM_{2.5}$ aqueous extracts of Coloradan urban and rural sources. Specifically, we studied the optical properties of the extracts (absorbance, fluorescence), their $^1O_2$ production, the $^{\bullet}OH$ sources and the effects of $^{\bullet}OH$ and non-$^{\bullet}OH$ pathways on the extract's characteristics during photoaging. Furthermore, as the gas phase $^{\bullet}OH$ transfer may be an important factor in the photoaging of $PM_{2.5}$ in the aqueous phase, a modelling exercise was done to compare the importance of the $^1O_2$ and $^{\bullet}OH$ condensed phase reaction to the $^{\bullet}OH$ gas phase transfer for a series of atmospheric relevant compounds.

2 Experimental

2.1 Sampling campaign

To explore the photoaging of $PM_{2.5}$ in the condensed phase, we used filter measurements of $PM_{2.5}$ collected from the Platte River Air Pollution and Photochemistry Experiment (PRAPPE).[19] PRAPPE sought to investigate various $PM_{2.5}$ characteristics and chemical transformations between three sites located along the Platte River; the sites were located in downtown Denver CO (urban), on a school roof in Platteville CO (mixed), and at the Jackson reservoir in eastern Colorado (rural), see Figure S1, supplementary information (SI) for the sites map and Figure S2, SI for wind roses. Atmospheric flow patterns along the front range have been studied extensively, aiding in our placement of the three sites.[20] Winds on average follow a diurnal atmospheric cycle. Notable for our study, radiative cooling of the land surfaces during the night causes downslope and eastern atmospheric transport, resulting in the night-time transportation of air closely following geographic features such as river valleys.[21, 22] The three sites act as sequential sampling locations that can explore $PM_{2.5}$ evolutions as it follows the Platte River out of Denver's urban cityscape and out toward the eastern plains. Three sampling campaigns were conducted, December 2016 (referenced later in the text as winter), February-March 2017 (referenced as spring) and July-August 2017 (referenced as summer). $PM_{2.5}$ samples were collected for 24 hours at 92 L min^{-1} on Teflon filters and frozen until further processing. Blank samples were generated the same way as the other samples except for the air pumps to be off during the sampling. See Table S1, SI for the PRAPPE filters data.

2.2 Extraction of the $PM_{2.5}$ filters

2.2.1 Extraction method

The Teflon filters collected during the sampling campaign were placed in individual Falcon tubes and extracted for 12 hours with 15ml of ultrapure water on a shaking table. The aqueous phase was then filtered on prewashed 0.45µm pore size polyethersulfone syringe filters. 2ml of the extracts were used for the soluble iron and the ionic content measurements, ≈2ml for the total organic carbon measurement and the rest of the extract for optical characterization and the photochemical experiments. To have more volume for the experiments, some extracts were diluted using ultrapure water to ≈30ml. Additionally, some of the extracts were combined. The dilution factor varied between 1.32-4.44, see Table S2, SI for the individual dilution factors and the extracts combinations. The extracts were frozen between the extraction and the photochemical experiments to prevent alteration. Blanks were processed in the same way as the other samples, see Table S3, SI for a comparison of some absorbance characteristics of the samples. The blanks absorbance values at 254 and 300nm were ≤ 10% of the mean absorbance value of the samples and the blanks $r_{\bullet OH}$ of ≈15% of the mean winter $r_{\bullet OH}$ (season with the lowest mean $r_{\bullet OH}$). The summer and springs extracts experiments were conducted mostly in duplicate while for the winter extracts the experiments were conducted once. Values presented for duplicates are the mean of the two measurements.

2.2.2 Calculation of the carbon extracted fraction

The fraction of the carbon extracted from the filters was calculated according to equation 9, where DOC_{ex} is the dissolved organic carbon (DOC) content of the aqueous extract ($mg_C\ L^{-1}$), V_{ex} is the amount of water used for the extraction (L), $EC+OC$ is the elemental + organic carbon concentration in the filtered air ($mg_C\ m^{-3}$) and V_{air} is the volume of air filtered (m^3).

$$Carbon\ Extraction\ efficiency\ /\ \% = \frac{DOC_{ex} \times V_{ex}}{(EC+OC) \times V_{air}} \quad (9)$$

2.3 Photoaging irradiation experiments

Photoirradiation experiments were conducted using an Oriel Sol1A solar simulator equipped with a 1000W xenon lamp and an air mass 1.5 filter. The UV-Visible spectral distribution of the lamp was measured using a wavelength calibrated Ocean Optics USB2000 spectrophotometer (Figure S3, SI). The extracts were irradiated for t=0, 12 or 24 hours in UV-transparent plastic cuvettes (see Figure S4, SI for a transmittance spectra of the cuvette) that were positioned at an angle of ≈30° from the horizontal in a temperature-controlled water bath (T= 20 ±1 °C). The daily irradiance of the lamp was measured during the first 5 hours of irradiation using a chemical actinometer (see below). To assess the influence of $^{\bullet}OH$ on the photoaging of the extracts, the irradiation experiments were repeated on the extracts in the presence of 0.1M methanol as a $^{\bullet}OH$ quencher.

The *p*-nitroanisol (PNA)/ pyridine actinometer[23] was used as described in the SI, Text S1. The reactive intermediates production rates were normalized using the daily measured PNA depletion rate to the average PNA rate ($1.68 \times 10^{-4}\ s^{-1}$). The photon fluence in the interval 290-400nm calculated using the average PNA depletion rate and the methods presented in Leresche et al.[16] is of 4.4×10^{-4} einstein $m^{-2}\ s^{-1}$. For comparison, the clear sky, noon photon fluence calculated for Boulder, Colorado in the 290-400nm interval is of 3.07×10^{-4} einstein $m^{-2}\ s^{-1}$ for the summer solstice, 2.61×10^{-4} einstein $m^{-2}\ s^{-1}$ for the equinoxes and 1.63×10^{-4} einstein $m^{-2}\ s^{-1}$ for the winter solstice.[24]

2.4 Measurements of photogenerated reactive intermediates

The methods used to quantify the production and quantum yields of $^1O_2$ and $^{\bullet}OH$ using probe compounds (furfuryl alcohol and benzoic acid respectively) are described elsewhere[16, 25, 26] and are additionally described in the SI, Texts S2 and S3.

2.5 Analytical instrumentations

Concentration of the probe compounds and of the actinometer were measured in duplicate on an Agilent 1200 HPLC system equipped with an Agilent Eclipse C-18 5µM particle size reversed phase column using the method described in the SI, Table S4. UV-Vis spectra were measured in quartz cuvettes (pathlength 1 or 5 cm) on a Cary 100 Bio UV-Visible spectrophotometer. The pH was measured with a calibrated Orion Star A211 pH-meter using a Thermo Scientific Orion pH electrode model 8157BNUMD. DOC was measured on a Sievers TOC analyser model M5310C. Fluorescence spectra were measured at room temperature using a Horiba Scientific FluoroMax-4 spectrofluorometer. The ionic content of the extracts was measured using inductively coupled plasma mass spectrometry (ICP-MS, Agilent 7700).

2.6 Chemicals

All solutions were prepared in ultrapure water (resistivity 18.2 MΩ cm) obtained from a Sartorios Stedim dispenser or equivalent. All chemicals were used as received except for benzoic acid that was recrystallized in ultrapure water and PNA in ethanol. For a complete list of chemicals please see the SI, Text S5.

3 Results and discussion

3.1 Characteristics of the extracts

The ionic content and some other characteristics such as the pH and DOC of the extracts are gathered in Table S2, SI. Probably due to the large range of values measured, the extracts mean characteristics appear to not vary significantly between the three sites, but some seasonal differences can be observed. The carbon extraction efficiency (according to equation 9) was found to vary between 5 and 32.2%, being relatively higher for the summer extracts than the winter extracts (27.8 ±2.5% vs 13.6 ±10.7%). The summer extracts DOC was also higher than winter and springs extracts DOC (11.8 ±1.6 vs 3.7 ±1.8 and 3.2 ±0.6 $mg_C\ L^{-1}$ respectively). It should be noted that the winter extracts were diluted after extraction and that without this dilution would have values higher than the springs extracts. Mean pH was lower for the summer (4.42) than for the spring (5.17) and winter (5.45) extracts. Nitrate was lower for the summer extracts (80±13 µM) than the winter extracts (122±95 µM) while mean iron concentration was higher (1.9±1.3 µM) for the summer extracts than for the winter (0.22±0.1 µM) extracts. For comparison, the PRAPPE filter data (before extraction) indicates that the average total iron concentration in the collected $PM_{2.5}$ were higher for the winter than the summer samples (107.3 vs 86.8 ng m^{-3}) but that the winter $PM_{2.5}$ iron was less soluble than the summer one (2.3 vs 9.9%).[19] The filters $PM_{2.5}$ were also seen to have an average iron concentration by sites that was higher for the urban (181.2 ng m^{-3}) than the mixed (76.1 ng m^{-3}) and rural filters (31.5 ng m^{-3}).

Some extracts optical characteristics are gathered in Table S3, SI. The specific UV-Vis absorbance at the wavelength λ=254 and 300nm ($SUVA_{254}$ and $SUVA_{300}$ respectively) have a mean value urban >mixed >rural. For surface waters, SUVA correlate with dissolved organic matter aromaticity,[27] indicating that the urban extracts probably have a higher aromatic substances content.

3.2 Effects of Photoirradiation on the Optical characteristics of the extracts

Absorbance

Simulated sunlight irradiation induced a decrease in the light absorbance of the extracts (see Figure 1). This decrease is more important for the wavelengths ≥ λ=300nm (see Figure S5, SI). For the wavelengths between 250 and 300 nm, a decrease in absorbance is observed upon irradiation for most of the extracts, while for part of the extracts irradiated in the presence of 0.1M methanol as an $^{\bullet}OH$ quencher, an increase is observed at short wavelength (λ≤300nm) (Figure 1, line 4).

Comparing the effects of 12 vs 24 hours of irradiation (Figure 1, line 2 vs 3), it can be observed that the decrease in absorbance is not linear with time but that the 12 first hours of irradiation induce a decrease in absorbance that is more important than the 12 subsequent hours of irradiation. Comparing the effects of 24 hours irradiation in the absence and in the presence of 0.1M methanol as a $^{\bullet}OH$ quencher (Figure 1, line 3 vs 4), it can be observed that the decrease in absorbance is larger in the absence of a $^{\bullet}OH$ quencher.

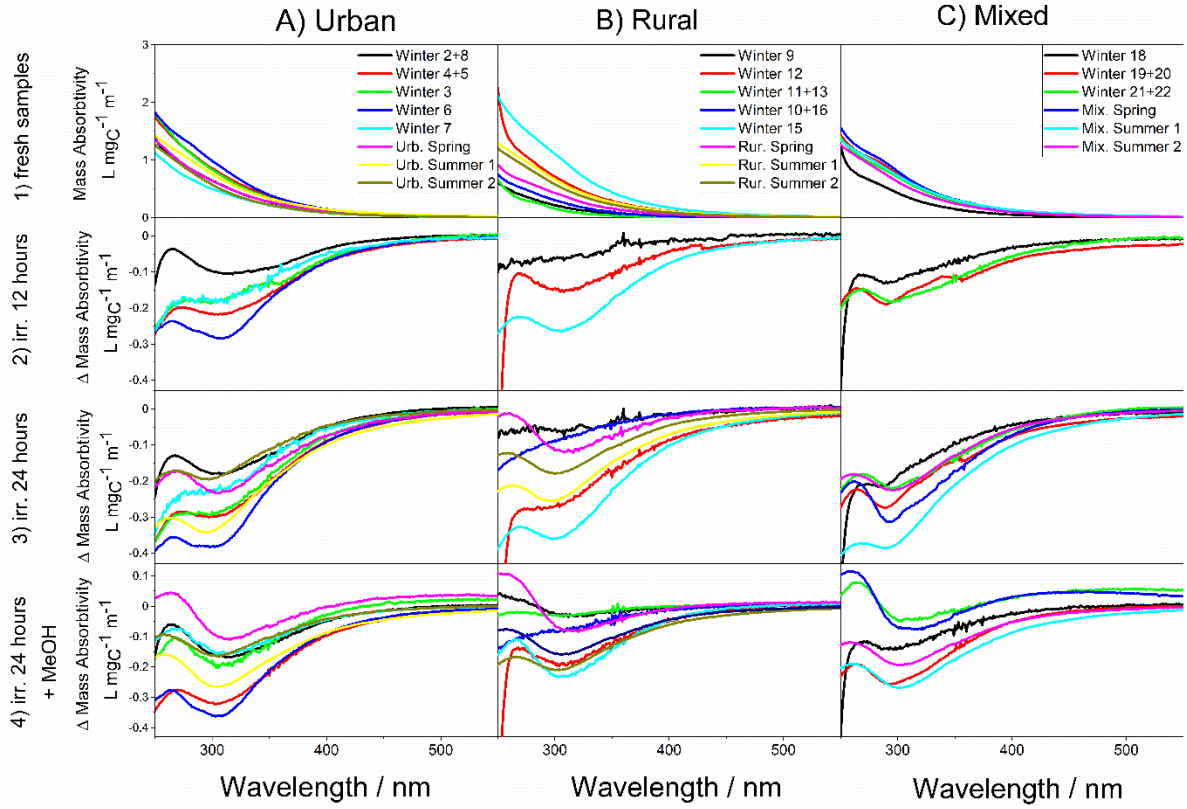

Figure 1, Optical characteristics of the $PM_{2.5}$ aqueous extracts and effects of photoaging in the presence and in the absence of 0.1M methanol as a hydroxyl radical (•OH) quencher. Line 1), mass absorptivity (MA= absorbance/[DOC]) of the fresh samples for the column A) urban samples, B) rural samples and C) mixed urban/rural samples. Line 2) variation ($MA_{i=12hours}$ - $MA_{i=0}$) of the mass absorptivity after 12 hours of simulated sunlight irradiation. Line 3) variation of the mass absorptivity ($MA_{i=24hours}$ - $MA_{i=0}$) after 24 hours of simulated sunlight irradiation. Line 4) variation of the mass absorptivity ($MA_{i=24hours, MeOH}$ - $MA_{i=0}$) after 24 hours of simulated sunlight irradiation in the presence of 0.1M methanol as a •OH quencher.

Literature reports indicates that photobleaching (i.e. a decrease in light absorbance) is the most common effect observed upon irradiation of secondary organic aerosols or of brown carbon in the aqueous phase.[5, 28-30] In some specific systems, an increase in absorption that is limited in time or for a limited wavelength range were observed.[9, 31-33] An example of such system is composed of secondary organic aerosols (SOA) prepared using chemical precursors.[31] The observed increase should be rationalized by the SOA having a composition dominated by a few compounds and the observed increase in absorbance to the formation of compounds that absorbs more for some specific wavelengths than the precursors. For the case of brown carbon nitrophenols, an observed initial increase in light absorbance was linked to •OH aromatic ring addition while further •OH exposure leads to loss in light absorbance due to the further reaction of the first addition products with •OH that lead to ring opening products and loss in absorbance properties.[34] The reduction in light absorbance properties observed in Figure 1 concurs

with the previous observations from literature, in that some of the extracts show a small gain in absorbance for a limited wavelength range, but more generally a loss in light absorbance properties is observed.

Two main mechanisms should rationalize the effects of photoirradiation on the optical properties of the extracts. The first effect is non-$^{\bullet}$OH reactions of chromophores and transformation to new moieties. The second effect is the reaction of a chromophores with $^{\bullet}$OH. From the photoirradiation experiments conducted in the absence or presence of a $^{\bullet}$OH quencher the influence of $^{\bullet}$OH and non-$^{\bullet}$OH pathways can be examined. It can be concluded that both $^{\bullet}$OH and non-$^{\bullet}$OH pathways contribute significantly to the photobleaching of the extracts. Note, the non-$^{\bullet}$OH pathways are expected to be direct photolysis and contribution of reactive species such as $^{1}O_2$ or ^{3}WSOC*.

Fluorescence

The fluorescence excitation emission matrices (EEMs) for the spring and summer extracts are presented in Figures S6 to S8, SI. The relative intensity (of the 24h aged samples to the fresh samples) for three features of the EEMs are presented in Figure 2 with the fluorescence quantum yield (Φ_F) while the corresponding data are collected in Table S5, SI. Note that three features are labeled as A, B and C. In surface waters, peak A (excitation/emission 300/414 nm) is associated to humic-like substances, peak B (excitation/emission 250/422 nm) to fulvic like substances, and peak C (excitation/emission 270/326 nm) to amino-acid like features.[35, 36] These assignments are questionable as for surface waters the fulvic acids fluorescence is more intense than the humic acids fluorescence, and that structures similar (e.g. phenols or indoles) to the fluorescing amino-acids (tryptophan and tyrosine) may be having similar fluorescence properties but are not necessarily amino-acids themselves.[37] We will hereafter describe the three features as peaks A, B and C.

On Figures 2 and S6-S8, SI it can be observed that the maximum fluorescence intensity value before irradiation is more important for the urban and mixed sample than the rural one. Photoirradiation induced a decrease of the fluorescence of the extracts with a 18-39% decrease of the peak A feature. This decrease was less important than the one observed (37-51%) for the irradiation conducted in the presence of 0.1M methanol as a $^{\bullet}$OH quencher. Photobleaching led to a stronger decrease in peak B relative to peak A. The photobleaching of peak B was not affected by the $^{\bullet}$OH quencher with value similar in the presence of the $^{\bullet}$OH quencher (35-54%) as in the absence (34-55%). Peak C is the most preserved feature that underwent only a moderate photobleaching (5-32%) in the absence of the $^{\bullet}$OH quencher while in the presence of the $^{\bullet}$OH quencher for some samples the fluorescence decreased while for some others an increase in fluorescence was observed (-21 to +38%). The Φ_F values for the urban samples were higher than the rural or mixed samples ones (see Figure 2D). Except for the mixed samples were Φ_F was left unchanged, irradiation induced a decrease in Φ_F, decrease that was larger for the samples irradiated in the presence of the $^{\bullet}$OH quencher than in the absence, observation that is interestingly the opposite as what is observed for the mass absorptivity of the samples (see Figure 1). As fluorophore are a fraction of the total number of chromophores, it can be hypothesized that the reaction of hydroxyl radical with chromophores produce new fluorophores.

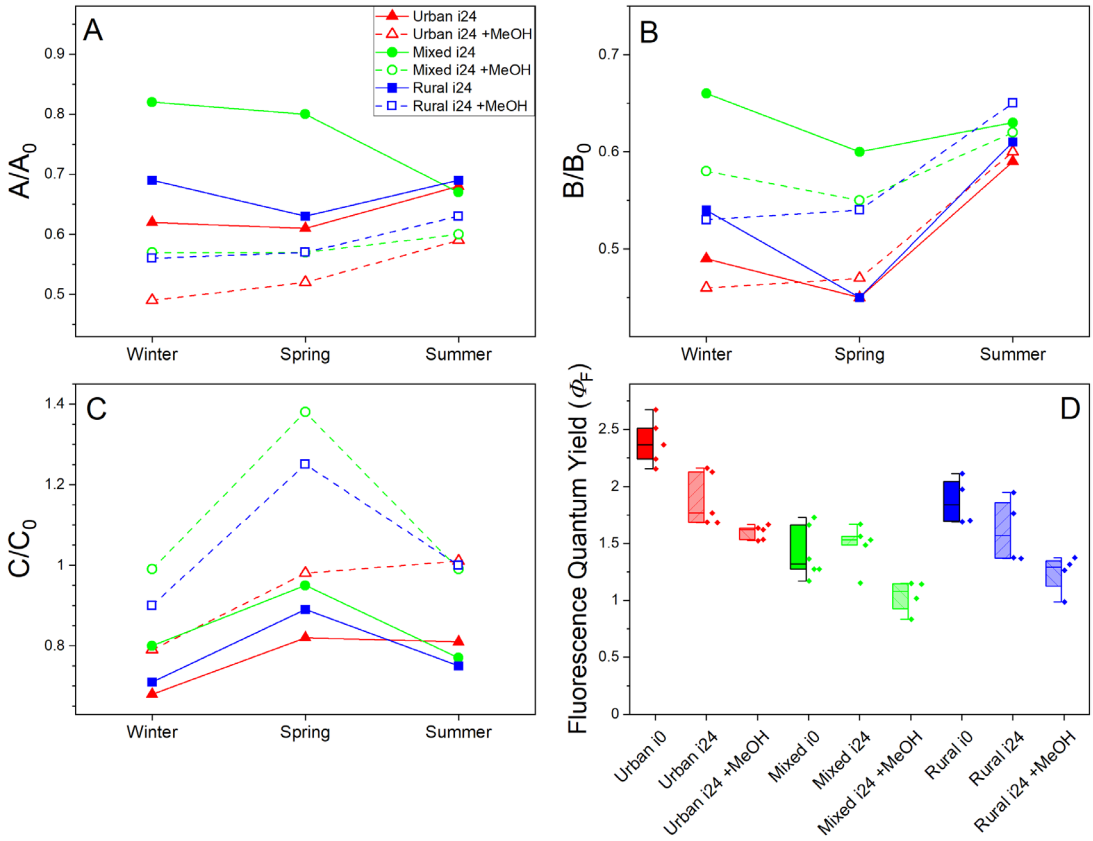

Figure 2, Effects of irradiation on the fluorescence peaks intensity and fluorescence quantum yields. A) Variation of peak A fluorescence (excitation 300nm/ emission 414nm) after 24h of irradiation relative to the fresh sample. B) Variation of peak B fluorescence (excitation 250nm/ emission 422nm). C) Variation of peak C fluorescence (excitation 270nm/ emission 326nm). Full symbols/continuous lines: Urban (red triangles), mixed (green circles) and rural (blue squares) samples. Hollow symbols/dashed lines: irradiation in the presence of 0.1M methanol as a $^{\bullet}$OH quencher. Lines are shown to guide the eye. D) Fluorescence quantum yield (Φ_F, %) box plots for the fresh, irradiated 24h, and irradiated 24 in the presence of 0.1M methanol as a $^{\bullet}$OH quencher. Red, urban samples. Green mixed samples. Blue, mixed samples. The data corresponding to Figure 2 is gathered in Table S5, SI.

Similar photoirradiation effect on EEMs on SOA produced from aromatic compounds precursors were observed with a decrease of the peak A feature.[31] Fluorescence signal > Em:350 nm has been generally associated to complex and conjugated aromatic molecules and light absorbing brown carbon.[38] These substances having important light absorption properties and high reactivity towards $^{\bullet}$OH (see introduction) should be both sensible to direct photolysis and of $^{\bullet}$OH reactions. As the decrease of intensity of peak A is seen to be equal or even more important in the presence of the $^{\bullet}$OH quencher, it can be hypothesized that reactions of $^{\bullet}$OH with WSOC may produce new fluorophores emitting at λ=414 nm intensifying the fluorescence of this

226 feature. The observed decrease in fluorescence of peak A in both irradiation experiments in the presence and in the absence of the $^{\bullet}$OH quencher indicates that photolysis altered the humic like substances present in the extract, photobleaching them.

228 Photoirradiation induces an important (35-54%) decrease in fluorescence on the peak B feature. As the simulated sunlight does not contain light for the wavelengths less than λ=300 nm (see Figure S1, SI), a first consideration could be that direct photolysis

230 should be excluded but as the decrease is observed in both the irradiation in the presence and in the absence of the $^{\bullet}$OH quencher it is actually likely that photolysis plays a major role in the disappearance of this feature and that these fluorophores absorb

232 additional light in the $\lambda \geq 300$ nm range.

For the $PM_{2.5}$ extracts irradiation experiments conducted in the presence of the $^{\bullet}$OH quencher, the fluorescence of the peak C

234 feature increased. It can be hypothesized that this increase in fluorescence is due to the formation of some photolysis product of WSOC and that in the presence of $^{\bullet}$OH this product would further react with $^{\bullet}$OH.

236 A decrease in Φ_F was observed for aquatic dissolved organic matter (DOM) samples and a DOM isolate,[17] where the Φ_F for the excitation wavelength λ=350nm was seen to decrease by ≈30-50% during 24 hours of irradiation. This observed trend is

238 similar or more important than the decrease in Φ_F observed here upon irradiation. The overall higher Φ_F values measured here for the urban site concurs with a scenario where the $PM_{2.5}$ collected in the urban site is fresher than the one collected on the

240 mixed and rural sites and were the $PM_{2.5}$ produced in the urban site is transported downwind to the mixed and rural sites. The trend observed on the SUVA values (see Table S3, SI), with SUVA urban >mixed >rural and the observed decrease in SUVA

242 values upon photoirradiation concords also with this scenario.

3.3 Generation potential of reactive intermediate species under irradiation

244 A detailed kinetic analysis of $^{\bullet}$OH reactivity towards WSOC is provided in Text S6 and Table S6, SI. The analysis indicates that the second-order rate constant $k_{\bullet OH,WSOC}$ of (4.9 ±2.3) $\times 10^{8}$ M_C^{-1} s^{-1} is comparable to the one of compounds such as benzoic

246 acid or acetaldehyde.

$^{\bullet}$OH radical production

248 Using the production of salicylic acid from the reaction of benzoic acid with $^{\bullet}$OH, the cumulative $^{\bullet}$OH production was measured as a function of time (see Figure 3 A and B). For the fresh urban and mixed summer samples, the cumulative $^{\bullet}$OH was seen to

250 level off with time (see Figure 3A). For all the other extracts, the cumulative $^{\bullet}$OH production was seen to have a good linearity on the experiment's timeframe (an example of such linearity is presented on Figure 3B).

252 The $^{\bullet}$OH production rates ($r_{\bullet OH}$) were calculated by fitting a zero-order kinetic rate to the data (for the fresh summer urban and mixed samples, the fit was done on the first ≈40 minutes). $r_{\bullet OH}$ were seen to be lower for the winter samples (mean = 4.8×10^{-12}

254 M s^{-1} mg_C^{-1} L) than for the spring samples (14.0×10^{-12} M s^{-1} mg_C^{-1} L) and the highest for the summer samples (65.4×10^{-12} M s^{-1} mg_C^{-1} L, see Figure 3C). The $r_{\bullet OH}$ of the fresh extracts as compared to the 24h photoaged extracts are very similar for the

256 winter and the spring samples with a mean $r_{\bullet OH}$ of 4.8×10^{-12} vs 4.3 $\times10^{-12}$ M s^{-1} mg_C^{-1} L (fresh vs 24h irradiated extracts) for the winter samples and a mean $r_{\bullet OH}$ of 14.0×10^{-12} M s^{-1} vs 14.5×10^{-12} M s^{-1} mg_C^{-1} L for the spring samples. Whereas a large

258 difference is observed for the summer extracts (mean $r_{\bullet OH}$ of 65.4×10^{-12} vs 6.4 $\times10^{-12}$ M s^{-1} mg_C^{-1} L) with a difference that is

more important for the urban and mixed sites (mean reduction of 87 and 93% upon 24h photoirradiation respectively) than for the rural site (mean reduction of 69%). The decrease in $r_{\bullet OH}$ observed for the summer extracts is probably due to the fast disappearance of a $^{\bullet}OH$ precursor pool (see below).

The $r_{\bullet OH}$ values can be compared to values observed for fog waters (14-77) $\times 10^{-12}$ M s^{-1} mg_C^{-1} L and values observed for rain water (17-64) $\times 10^{-12}$ M s^{-1} mg_C^{-1} L.[11, 39] The comparison indicates that the values observed here for the winter extracts are lower than what is observed for the fog and rain waters, the springs extracts compare to the lower values and the summer extracts to the higher values observed for the fog and rain waters.

On Figure 3D, the winter extracts $r_{\bullet OH}$ is presented as a function of the nitrate concentration. It can be observed that there is a relatively good linear correlation between $r_{\bullet OH}$ and nitrate concentration (except for the urban samples). Control experiments measuring $r_{\bullet OH}$ from sodium nitrate photolysis in ultrapure water indicates that nitrate is one of the main sources of $^{\bullet}OH$ for the winter extracts (Figure 3D). In opposition, nitrate can be seen to be only a minor source of $^{\bullet}OH$ for the summer extracts (Figure S9A, SI). On the other potential sources of $^{\bullet}OH$ in the summer extracts (see introduction), nitrite can also be seen to be a minor source of $^{\bullet}OH$ (Figure S9B, SI) while for iron a linear correlation exists between the $^{\bullet}OH$ and the iron concentration of the extracts ($R^2 = 0.36$, Figure S9C, SI) indicating that iron may play a role in the $^{\bullet}OH$ production of the summer extracts.

The sources of $^{\bullet}OH$ in the extracts are believed to be mostly nitrate, nitrite, iron (via the Fenton and photo-Fenton reaction) and WSOC irradiation. From the nitrate and nitrite photolysis control experiments, assuming that every $^{\bullet}OH$ correspond to the disappearance of one molecule of nitrate or nitrite respectively during these control experiments, one can calculate the half-life ($t_{1/2}$) of nitrate and nitrite to be of 119 days and of 7.5 hours respectively ($t_{1/2} = \ln 2 / k$). During the course of one irradiation experiments (24h), $r_{\bullet OH}$ from nitrate photolysis is stable while $r_{\bullet OH}$ from nitrite photolysis should decrease by a factor ≈8. The nitrite lifetime value corresponds to a value reported in the literature of 5.4 hours but the nitrate value is one order of magnitude longer that the value reported in the literature of 10.5 days.[40] The reason for this difference is not clear but a possible explanation would be the solar simulator having a lower UV irradiance than the value calculated for 40°N during the summer of Zellner et al.[40]

The $^{\bullet}OH$ produced from WSOC photoirradiation should be proportional to the amount of light absorbed, with eventually an initial phase of increased $^{\bullet}OH$ produced from fast disappearing chromophores at the beginning of the irradiation. Such behaviour was recently observed on the ≈2minutes irradiation timescale and was attributed to a Fenton-like decomposition of peroxy acids,[41] the timescale of the decrease in $r_{\bullet OH}$ observed here for the fresh urban and mixed samples is relatively longer (≈1 hour, see Figure 3A) but this could be due to kinetic reasons such as the pH being higher in the present experiments (4.42 for the summer samples vs 3.5). The Fenton and photo-Fenton reaction can potentially lead to $r_{\bullet OH}$ rates that would decrease with time and explain the observed results (see reactions 5 and 6). This should be expected if the iron speciation shift with time if iron ligand complexes are photodegraded leading to a modified iron reactivity or if some precursors such as peroxy acids are decomposed. A trend generally observed is that the fraction of iron (II) is higher during daytime than during night-time, a photochemical exhaustion of iron(III) in the aqueous extract is possible and could lead to the observed fast reduction of $r_{\bullet OH}$ for the summer urban and mixed samples, these samples being the ones with the highest soluble iron concentration.[19]

Salazar et al. hypothesized that the source of the higher iron concentration in the summer samples is pyrogenic.[19] The observed decrease in $r_{\bullet OH}$ observed for the fresh urban and mixed samples could be photo labile pyrogenic chromophores.

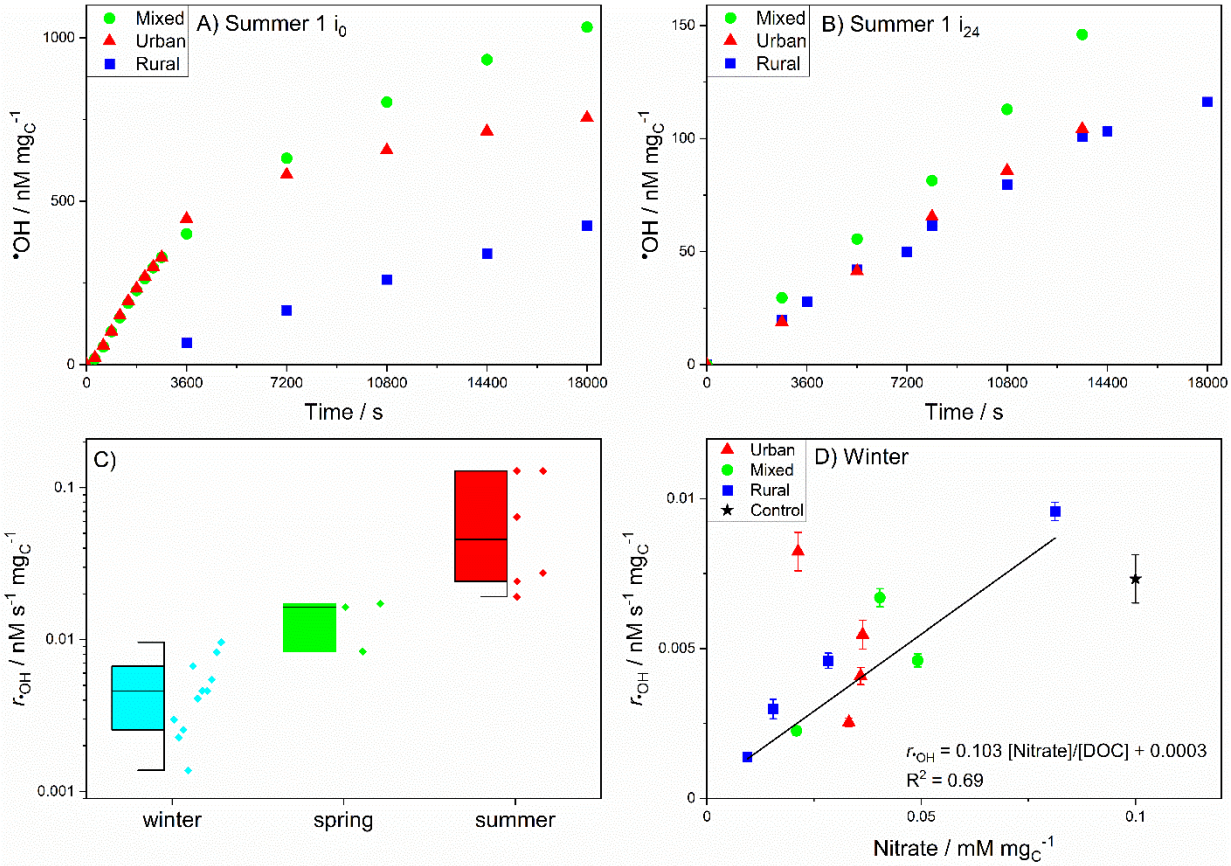

Figure 3, Production of hydroxyl radicals (•OH) of the $PM_{2.5}$ aqueous extracts. A) Cumulative •OH production vs time for the summer 1 fresh samples. Red triangles: urban, green circles: mixed and blue squares: rural samples. B) Cumulative •OH production vs time for the summer 1 24h-irradiated samples. C) Box plots of the fresh samples rate of •OH production ($r_{\bullet OH}$) for the winter (cyan), spring (green) and summer (red) extracts. D) Rate of •OH production ($r_{\bullet OH}$) as a function of the nitrate concentration for the winter extracts, black stars represent $r_{\bullet OH}$ of the nitrate control experiments in ultrapure water (nitrate control: x-unit nM, y-unit nM s^{-1}). The black linear regression line excluded the data from the nitrate control experiments.

Intrinsic •OH production vs gas phase •OH diffusion

The main source of •OH in atmospheric droplets is believed to usually be transfer from the gas phase. For 10µm diameter water droplets and a gaseous [•OH] of 1.1×10^6 molecules cm^{-3}, the uptake of •OH was estimated to be of 2×10^{-9} M s^{-1}.[41] The condensed phase production of •OH (i.e. $r_{\bullet OH}$) can be compared to this gas phase transfer rate. The mean summer, spring and winter $r_{\bullet OH}$ are of respectively 0.065×10^{-9} , 0.014×10^{-9} and 0.004×10^{-9} M s^{-1} mg_C^{-1} L, multiplying these values by the mean WSOC concentration 11.5 mg_C L^{-1} for fog waters found in Kaur and Anastasio[11], it is possible to calculate that the condensed

phase values represents respectively 38%, 8% and 2.7% of the gas phase $^{\bullet}OH$ uptake, indicating that for summer extracts both the condensed phase and gas phases uptakes are important source of aqueous $^{\bullet}OH$ while for the spring and winter extracts the gas phase uptake is the main source of aqueous $^{\bullet}OH$.

Sinks of $^{\bullet}OH$ in the extracts

For atmospheric droplets, it has been shown that in the aqueous phase the main sink of $^{\bullet}OH$ is reaction with WSOC and the inorganic content of the droplets while $^{\bullet}OH$ transfer to the gas phase is in comparison low.[41] We will here neglect it and only consider the condensed phase $^{\bullet}OH$ reactions as sinks.

The fraction f_i of $^{\bullet}OH$ reacting with a specific extract component can be calculated by using equation 10, where $k_{Q_i,\bullet OH}$ is the second-order rate constant between $^{\bullet}OH$ and the species Qi and [Qi] the concentration of the species Qi.

$$f_i = \frac{k_{Q_i,\,\bullet OH}\,[Q_i]}{\sum k_{Q_i,\,\bullet OH}\,[Q_i]} \qquad (10)$$

It should be noted that equation 10 is valid for irreversible reactions. For bromide and chloride reactions, their reaction with $^{\bullet}OH$ are mostly reversible and the rate constant used was calculated using the pre-equilibrium approximation (see Text S7, SI). Reactions of chloride and bromide with $^{\bullet}OH$ should produce small quantities of radicals such as $Br^{\bullet}$, $Br_2^{\bullet-}$, $Cl^{\bullet}$ and $Cl_2^{\bullet-}$.[42, 43] Using $k_{\bullet OH,WSOC}$ of $(4.9 \pm 2.3)\times10^{8}$ M_C^{-1} s^{-1} (mean fog and cloud waters value from Arakaki et al.[44]. Note, the second-order rate constant has to be expressed in M_C^{-1} s^{-1} unit due to the unknown WSOC molar mass, see also Text S6, SI) and the second-order constants of $^{\bullet}OH$ towards inorganics ions from Buxton et al.[45] we calculated that for the summer extracts, most (≈89%) of the produced $^{\bullet}OH$ reacted with the WSOC (see Table S7 and S8, SI) while nitrite and bromide were minor sinks of $^{\bullet}OH$.

The $^{\bullet}OH$ steady-state concentration ($[^{\bullet}OH]_{ss}$) can be calculated according to equation 11, where the denominator is the same as in equation 10:

$$[\,^{\bullet}OH\,]_{ss} = \frac{r_{\bullet OH}\,[WSOC]}{\sum k_{Q_i,\,\bullet OH}\,[Q_i]} \qquad (11)$$

Using equation 11, the mean $[^{\bullet}OH]_{ss}$ for the summer extracts, considering only the aqueous $r_{\bullet OH}$ production, is 1.4×10^{-15} M, a value that is WSOC concentration independent. Adding to the condensed phase $r_{\bullet OH}\times[WSOC]$, the gas transfer rate of 2×10^{-9} M s^{-1}, the $[^{\bullet}OH]_{ss}$ value is 5.2×10^{-15} M. Both values are relatively higher than values that did not included gas transfer observed for a series of laboratory generated secondary organic aerosols extracts $(2.6\text{-}4.9)\times10^{-17}$ M and of PM smaller than 10 µm (PM_{10}) extracts collected in fall and spring in rural Switzerland $(2.3\text{-}3.3)\times10^{-17}$ M [12] or the values observed for a series of fog extracts under winter solstice solar irradiation condition $(3.4\text{-}11)\times 10^{-16}$ M.[11]

$^{\bullet}OH$ effects on the Absorbance

The ratio of the absorbance after 24 hours irradiation over the initial absorbance is presented for the wavelength λ=254nm and 330 nm vs $r_{\bullet OH}$ (Figure 4A and B). It can be observed that for λ=254nm the decrease in absorbance is relatively similar between the extracts with, for the summer sample, a good correlation (R^2 = 0.84) with $r_{\bullet OH}$ (Figure 4A) while for the wavelength

λ=330nm, the ratio A/A_0 is overall lower and that a better linear correlation for the summer samples (R^2 = 0.87) exists with $r_{\bullet OH}$ (Figure 4B). It should be noted that examination of the full absorbance spectra indicates that photoirradiation induces a decrease in absorbance at λ=330nm for all samples while for the wavelengths shorter than λ=300nm an increase in absorbance is observed for some extracts (Figure 1). Boxplot charts of A/A_0 for the three sampling sites and for the irradiation experiments in the absence and presence of 0.1M methanol as a $^{\bullet}OH$ quencher reveal that the decrease in absorbance is lower for the irradiation in the presence of the $^{\bullet}OH$ quencher both for the wavelength of λ=254nm and for λ=330nm (Figure 4C and D) and that for a few extracts at λ=254nm an increase in absorbance is observed (Figure 4C).

The linear relationship observed at λ=330nm has an ordinate of 0.60 that indicates that most of the decrease in absorbance at this wavelength should be attributed to non-$^{\bullet}OH$ radical pathways, Figure 4D indicates that this is indeed the case as the presence of the $^{\bullet}OH$ quencher influences only moderately the decrease in absorbance. The observed linear relationship at λ=330nm indicates that for the extracts having an important $r_{\bullet OH}$ (i.e. mostly summer extracts), $^{\bullet}OH$ also plays an important role in the absorbance decrease.

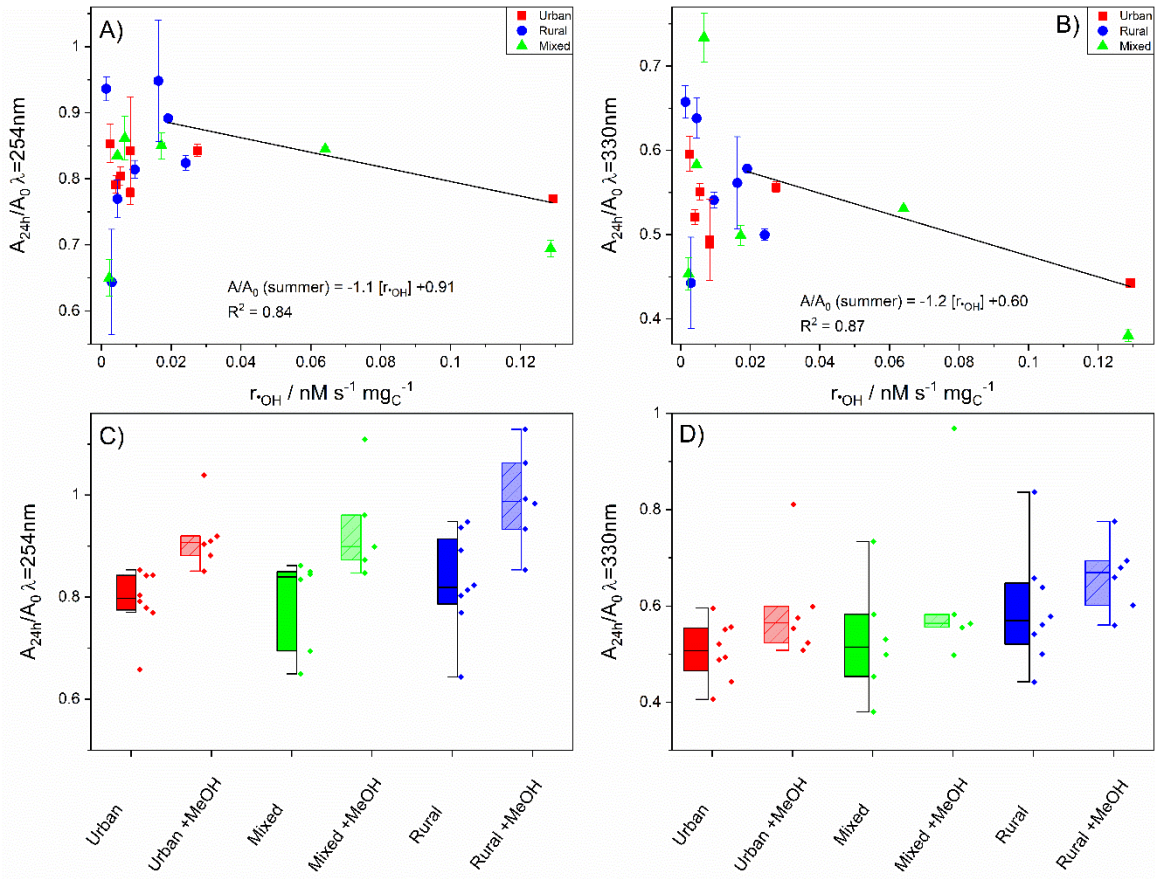

Figure 4, Effects of hydroxyl radicals ($^{\bullet}OH$) on the optical properties of the $PM_{2.5}$ aqueous extracts. A) and B) Relative (to the fresh samples) variation of the absorbance after 24hours simulated sunlight irradiation of the $PM_{2.5}$ extracts for the wavelength λ=254nm (A) and λ=330nm (B) as a function of the rate of $^{\bullet}OH$ production ($r_{\bullet OH}$). Red squares: urban, green triangles: mixed and blue circles: rural samples. Black lines are linear regression lines for the summer samples (note, the summer samples are the six samples with the highest $r_{\bullet OH}$ on both subfigure A and B). C) and D), boxplots of the relative (to the fresh samples) variation of the absorbance at λ=254nm (C) and λ=330nm (D) after 24hours for the urban (red), mixed (green) and rural (blue) extracts in the absence (full boxes) and presence (dashed boxes) of 0.1 M methanol as a $^{\bullet}OH$ quencher.

Singlet oxygen ($^1O_2$)

For a subset of samples, we examined the production of $^1O_2$ and calculated the singlet oxygen steady-state concentration ($[^1O_2]_{ss}$) and quantum yield (Φ_{1O2}). As $[^1O_2]_{ss}$ is [WSOC] dependent,[15] the $[^1O_2]_{ss}$ were normalized to a [WSOC] of 11.5mg$_C$ L^{-1}. The results are presented in Table S9, SI where $[^1O_2]_{ss}$ can be seen to be systematically higher for the fresh extracts (mean value 19×10^{-14} M) and relatively similar between the extracts irradiated in the absence and in the presence of the $^{\bullet}OH$ quencher (9.6×10^{-14} vs 9.7×10^{-14} M). The Φ_{1O2} are similar between fresh and irradiated in the absence of the $^{\bullet}OH$ quencher extracts (mean of 3.7 and 3.1%) but relatively lower for the irradiated extracts in the presence of the $^{\bullet}OH$ quencher (2.2%).

The range of observed $[^1O_2]_{ss}$ is relatively similar than the ones observed in previous studies for fog water ((0.11-3) $\times10^{-13}$ M)[11] and ((1.1-6.1) $\times10^{-13}$ M)[46] but higher than what was observed for rainwaters (2.7 $\times10^{-15}$ - 2.4 $\times10^{-21}$ M)[39] and for SOA extracts ((1.1-4.5) $\times10^{-14}$ M) and two PM_{10} extracts ((0.8-1.4) $\times10^{-14}$ M).[12] For Φ_{1O2}, previous studies indicate that there is quite some variation of Φ_{1O2} with the WSOC sources with values for fog water of 0.4-12%,[11] for SOA extracts of 0.3-3 % and of 4-4.5% for two PM_{10} extracts[12] while a value of 33% was observed for a dissolved soot extract.[47] These observed values likely reflects the variation in composition and age of the aerosol WSOC and agree with the present observations.

$[^1O_2]_{ss}$ vs $[^{\bullet}OH]_{ss}$

Comparing $[^1O_2]_{ss}$ with $[^{\bullet}OH]_{ss}$, it can be calculated that $[^1O_2]_{ss}$ has a mean concentration 261 higher for the summer samples than $[^{\bullet}OH]_{ss}$ when the condensed phase production of $^{\bullet}OH$ is considered (Table S9, SI). When a gas transfer rate of 2×10^{-9} M s^{-1} is added to the aqueous $r_{\bullet OH}$, it can be calculated that the ratio $[^1O_2]_{ss}/[^{\bullet}OH]_{ss}$ has a mean value of 26. For a given compound, it is possible to compare its reactivity towards $^1O_2$ and $^{\bullet}OH$ by multiplying its corresponding second-order rate constant towards $^1O_2$ or $^{\bullet}OH$ by $[^1O_2]_{ss}$ or $[^{\bullet}OH]_{ss}$ respectively. Note, a limitation of this comparison is that $[^1O_2]_{ss}$ is WSOC concentration dependent while $[^{\bullet}OH]_{ss}$ is not.[48] This may make the ratio $[^1O_2]_{ss}/[^{\bullet}OH]_{ss}$ dependent on WSOC concentration. A second limitation is that the gas transfer rate is proportional to the surface of the droplets while the condensed phase $^1O_2$ and $^{\bullet}OH$ production is proportional to the droplets volume, this makes the ratio condensed phase $^{\bullet}OH$ production /gas $^{\bullet}OH$ transfer dependent on the droplet diameter.

For a series of compounds, we calculated that ratio using either the condensed phase $[^{\bullet}OH]_{ss}$ or the heterogeneous $[^{\bullet}OH]_{ss}$. The results are presented as f_{1O2} in Figure 5A (while the data is gathered in Table S10, SI), where f_{1O2} is the fraction of the compound

that reacts with $^1O_2$ that can be calculated using equation 12, where $k_{\bullet OH,P}$ and $k_{1O2,P}$ are the second-order rate constants of the compound P towards $^\bullet OH$ or $^1O_2$ respectively.

$$f_{1O2} = \frac{k_{1O2,P}[\,^1O_2]_{ss}}{k_{1O2,P}[\,^1O_2]_{ss} + k_{\bullet OH,P}[\,^\bullet OH]_{ss}} \quad (12)$$

The f_{1O2} values vary from 4.1×10^{-5} to 0.61 for the condensed phase system and from 1.1×10^{-5} to 0.29 for the heterogeneous system with mean values of 0.15 and 0.063 respectively. The compounds that have a f_{1O2} value higher than 10% all have a high reactivity ($k_{\bullet OH,P} > 1\times10^9$ M^{-1} s^{-1}) towards $^\bullet OH$ and also a high reactivity ($k_{1O2,P} > 2\times10^7$ M^{-1} s^{-1}) towards $^1O_2$. The compounds that have a reactivity towards $^\bullet OH$ close to the one of WSOC with a $k_{\bullet OH,P} < 1\times10^9$ M^{-1} s^{-1} (see above) all have a f_{1O2} values below 5%. It can be concluded so that for the mean WSOC component $^1O_2$ does not contribute significantly to their disappearance compared to $^\bullet OH$ for conditions similar to the one of the presents experiments.

Knowing $[^1O_2]_{ss}$ and $[^\bullet OH]_{ss}$ and the second-order rate constant of a compound P toward $^\bullet OH$ and $^1O_2$ ($k_{\bullet OH,P}$ and $k_{1O2,P}$ respectively), it is also possible to calculate the compounds disappearance rate due to $^1O_2$ or $^\bullet OH$ using equation 13:

$$-\frac{dP}{dt} = P\,(k_{1O2,P}[\,^1O_2]_{ss} + k_{\bullet OH,P}[\,^\bullet OH]_{ss}) \quad (13)$$

This value is reported on Figure 5 for a series of compound as their corresponding half-lives ($t_{1/2}$) that can be calculated using equation 14:

$$t_{1/2} = \frac{\ln 2}{k_{1O2,P}[\,^1O_2]_{ss} + k_{\bullet OH,P}[\,^\bullet OH]_{ss}} \quad (14)$$

It should be noted that these half-lives values are calculated neglecting other possible reactions (e.g. direct photolysis or ^{3}WSOC* oxidation) of a compound. They should be so considered as upper limit maximum. Some of the selected compounds are known to be subject to direct photolysis (e.g. 4-nitrophenol[49]) or in surface waters to ^{3}DOM* induced phototransformation (e.g. phenol[50] or methionine[51]) and their lifetime should be shorter than the results presented here.

The $t_{1/2}$ values vary from 6.9 to 1612 hours for the values calculated using the condensed phase $[^1O_2]_{ss}$ or $[^\bullet OH]_{ss}$ values while they vary from 1.9 to 434 hours for the heterogeneous system. The lowest $t_{1/2}$ values being for cysteine while the highest values for acetate.

The ratio $[^1O_2]_{ss}/[^\bullet OH]_{ss}$ is probably dependent on the irradiation spectra. As the sunlight spectra varies with the atmospheric condition,[52] the ratio is also probably dependent of the atmospheric conditions. Examination of such influence is beyond the scope of this paper. It should also be noted that 1,4-benzoquinone, the compound having the highest calculated f_{1O2} value have recently been detected in wildfire smoke,[53] indicating that in certain instances $^1O_2$ could significantly contributes to the phototransformation of atmospheric components in the aqueous phase.

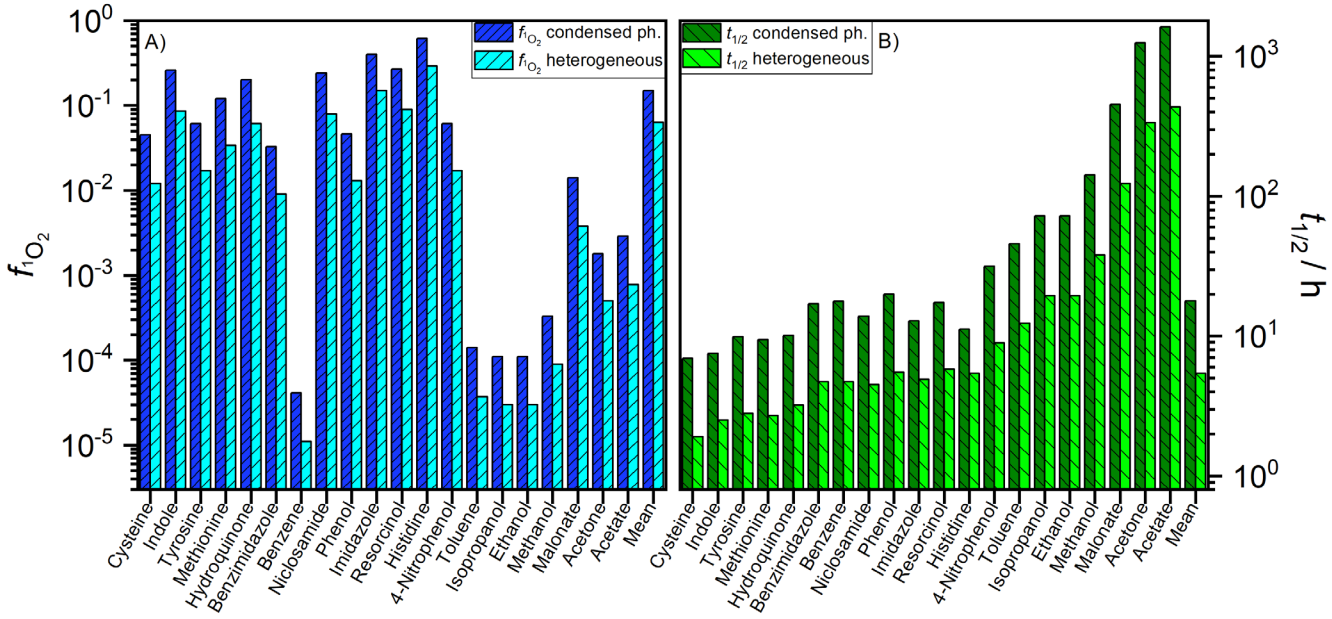

Figure 5, (A) Fraction of the reactivity towards singlet oxygen (f_{1O2}) for a series of compounds and (B) their corresponding half-lives ($t_{1/2}$) in the atmospheric aqueous phase.

Environmental implications

To understand the implications of this work, we must first understand how important the gas transfer rate is compared to the condensed phase reactions for the aging of $PM_{2.5}$ in the atmospheric aqueous phase. Two conditions that influence the gas transfer and the condensed phase reactions are: 1) the size of the droplets and 2) WSOC concentration. For 1, the ratio condensed phase / gas transfer is proportional to the droplet's diameter (see above). For 2, $[^1O_2]_{ss}$ is proportional to [WSOC] while $[^{\bullet}OH]_{ss}$ is [WSOC] independent considering only the condensed phase reaction and if one considers also the gas transfer $[^{\bullet}OH]_{ss}$ is inversely proportional to [WSOC] (one can add a gas transfer term to the numerator of equation 11 to calculate that). A high [WSOC] would so increase $[^1O_2]_{ss}$ while decreasing $[^{\bullet}OH]_{ss}$.

One observation made in this article is that nitrate photolysis (equation 4) was the dominant source of $^{\bullet}OH$ for the winter extracts (Figure 3) but that the winter condensed phase $r_{\bullet OH}$ represented only 2.7% of the gas transfer rate, indicating that nitrate photolysis is negligible in the experimental conditions. Conditions where nitrate photolysis could be an important $^{\bullet}OH$ source would be bigger size droplets, higher nitrate concentration, lower [WSOC], and days with increased UV-fluence. UV-part of the solar spectra being its most variable part.[52] For the summer extracts, $r_{\bullet OH}$ was on the same order of magnitude (38%) compared to the gas transfer rate. For the urban and mixed samples $r_{\bullet OH}$ decreased with irradiation time. A correlation was seen between the summer extracts $r_{\bullet OH}$ and iron concentration indicating that the Fenton and photo-Fenton reaction (equation

5 and 6) are probably an important source of $^{\bullet}OH$ for those samples. The presence of a $^{\bullet}OH$ quencher influenced only moderately the decrease in absorbance upon photoirradiation (see Figure 4), indicating that non-$^{\bullet}OH$ significantly contributed to the photobleaching of the extracts. The modelling exercise indicated that $^1O_2$ would contribute significantly to the disappearance of high-reactivity ($k_{1O2,P}$ >2×10^7 M^{-1} s^{-1}) compounds. The contribution of ^{3}WSOC* was neglected in the modeling, as in surface waters excited triplet state of DOM (^{3}DOM*) can be seen to be a more important contributor than $^1O_2$ for some micropollutants,[54] ^{3}WSOC* most probably contributes significantly to the transformation of some compounds in the atmospheric aqueous phase. A factor that may warrant more attention is that with the aerosols aging, the mean WSOC second-order rate constant towards reactive species is decreasing, a decrease that is probably more important for the selective oxidant ($^1O_2$, ^{3}WSOC*) than for $^{\bullet}OH$. E.g., for the compounds presented in Figure 5, the mean second-order rate constant of the 4 most reactive compounds towards $^1O_2$ is of 4.5×10^7 M^{-1} s^{-1} vs 2.1×10^3 M^{-1} s^{-1} for the 4 least reactive while for the same compounds their mean $^{\bullet}OH$ second-order rate constant is of 9.0×10^9 M^{-1} s^{-1} vs 1.0×10^9 M^{-1} s^{-1}.

Acknowledgements

Funding for this study came from the US National Science Foundation (Grant No. 1549387). The authors would like to thank Sarah J. Fischer for her useful comments on the fluorescence properties of the extracts and three anonymous reviewers for their helpful comments on the manuscript.

Associated Content

Supporting Information

The Supporting Information is available free of charge at:…

Tables, texts and Figures with the sampling campaigns information, characteristics of the aqueous extracts, HPLC methods, list of chemicals used in the experiments, pre-equilibrium approximation kinetic model, reaction of $^{\bullet}OH$ with the extract's components and additional data, figures and tables.

Author information

Corresponding author

*E-mail: Frank.Leresche@colorado.edu

ORCID

Frank Leresche: 0000-0001-8400-3142

Joseph R. Salazar:

David J. Pfotenhauer: 0000-0001-7336-3900

Michael P. Hannigan: 0000-0002-9877-9459

Brian J. Majestic: 0000-0003-1860-8738

Fernando Rosario-Ortiz: 0000-0002-3311-9089

Note

The authors declare no competing financial interest.

References

1. Nel, A., Air pollution-related illness: Effects of particles. *Science* **2005,** *308* (5723), 804-806.
2. Ramanathan, V.; Carmichael, G., Global and regional climate changes due to black carbon. *Nature Geoscience* **2008,** *1* (4), 221-227.
3. Bond, T. C.; Bergstrom, R. W., Light absorption by carbonaceous particles: An investigative review. *Aerosol Science and Technology* **2006,** *40* (1), 27-67.
4. Jimenez, J. L.; Canagaratna, M. R.; Donahue, N. M.; Prevot, A. S. H.; Zhang, Q.; Kroll, J. H.; DeCarlo, P. F.; Allan, J. D.; Coe, H.; Ng, N. L.; Aiken, A. C.; Docherty, K. S.; Ulbrich, I. M.; Grieshop, A. P.; Robinson, A. L.; Duplissy, J.; Smith, J. D.; Wilson, K. R.; Lanz, V. A.; Hueglin, C.; Sun, Y. L.; Tian, J.; Laaksonen, A.; Raatikainen, T.; Rautiainen, J.; Vaattovaara, P.; Ehn, M.; Kulmala, M.; Tomlinson, J. M.; Collins, D. R.; Cubison, M. J.; Dunlea, E. J.; Huffman, J. A.; Onasch, T. B.; Alfarra, M. R.; Williams, P. I.; Bower, K.; Kondo, Y.; Schneider, J.; Drewnick, F.; Borrmann, S.; Weimer, S.; Demerjian, K.; Salcedo, D.; Cottrell, L.; Griffin, R.; Takami, A.; Miyoshi, T.; Hatakeyama, S.; Shimono, A.; Sun, J. Y.; Zhang, Y. M.; Dzepina, K.; Kimmel, J. R.; Sueper, D.; Jayne, J. T.; Herndon, S. C.; Trimborn, A. M.; Williams, L. R.; Wood, E. C.; Middlebrook, A. M.; Kolb, C. E.; Baltensperger, U.; Worsnop, D. R., Evolution of Organic Aerosols in the Atmosphere. *Science* **2009,** *326* (5959), 1525-1529.
5. Ray, D.; Ghosh, S. K.; Raha, S., Impacts of some co-dissolved inorganics on in-cloud photochemistry of aqueous brown carbon. *Atmospheric Environment* **2020,** *223,* 117250.
6. Birmili, W.; Allen, A. G.; Bary, F.; Harrison, R. M., Trace metal concentrations and water solubility in size-fractionated atmospheric particles and influence of road traffic. *Environmental Science & Technology* **2006,** *40* (4), 1144-1153.
7. Daumit, K. E.; Carrasquillo, A. J.; Sugrue, R. A.; Kroll, J. H., Effects of Condensed-Phase Oxidants on Secondary Organic Aerosol Formation. *Journal of Physical Chemistry A* **2016,** *120* (9), 1386-1394.
8. Walhout, E. Q.; Yu, H. M.; Thrasher, C.; Shusterman, J. M.; O'Brien, R. E., Effects of Photolysis on the Chemical and Optical Properties of Secondary Organic Material Over Extended Time Scales. *ACS Earth and Space Chemistry* **2019,** *3* (7), 1226-1236.
9. Zhao, R.; Lee, A. K. Y.; Huang, L.; Li, X.; Yang, F.; Abbatt, J. P. D., Photochemical processing of aqueous atmospheric brown carbon. *Atmospheric Chemistry and Physics* **2015,** *15* (11), 6087-6100.
10. Arakaki, T.; Kuroki, Y.; Okada, K.; Nakama, Y.; Ikota, H.; Kinjo, M.; Higuchi, T.; Uehara, M.; Tanahara, A., Chemical composition and photochemical formation of hydroxyl radicals in aqueous extracts of aerosol particles collected in Okinawa, Japan. *Atmospheric Environment* **2006,** *40* (25), 4764-4774.
11. Kaur, R.; Anastasio, C., Light absorption and the photoformation of hydroxyl radical and singlet oxygen in fog waters. *Atmospheric Environment* **2017,** *164*, 387-397.
12. Manfrin, A.; Nizkorodov, S. A.; Malecha, K. T.; Getzinger, G. J.; McNeill, K.; Borduas-Dedekind, N., Reactive Oxygen Species Production from Secondary Organic Aerosols: The Importance of Singlet Oxygen. *Environmental Science & Technology* **2019,** *53* (15), 8553-8562.
13. Kaur, R.; Anastasio, C., First Measurements of Organic Triplet Excited States in Atmospheric Waters. *Environmental Science & Technology* **2018,** *52* (9), 5218-5226.
14. Vione, D.; Minella, M.; Maurino, V.; Minero, C., Indirect photochemistry in sunlit surface waters: photoinduced production of reactive transient species. *Chemistry - A European Journal* **2014,** *20* (34), 10590-10606.
15. McNeill, K.; Canonica, S., Triplet state dissolved organic matter in aquatic photochemistry: Reaction mechanisms, substrate scope, and photophysical properties. *Environmental Science: Processes & Impacts* **2016,** *18*, 1381-1399.
16. Leresche, F.; McKay, G.; Kurtz, T.; von Gunten, U.; Canonica, S.; Rosario-Ortiz, F. L., Effects of Ozone on the Photochemical and Photophysical Properties of Dissolved Organic Matter. *Environmental Science & Technology* **2019,** *53* (10), 5622-5632.
17. Del Vecchio, R.; Blough, N. V., Photobleaching of chromophoric dissolved organic matter in natural waters: kinetics and modeling. *Marine Chemistry* **2002,** *78* (4), 231-253.
18. White, E. M.; Vaughan, P. P.; Zepp, R. G., Role of the photo-Fenton reaction in the production of hydroxyl radicals and photobleaching of colored dissolved organic matter in a coastal river of the southeastern United States. *Aquatic Sciences* **2003,** *65* (4), 402-414.

19. Salazar, J. R.; Pfotenhauer, D. J.; Leresche, F.; Rosario-Ortiz, F. L.; Hannigan, M. P.; Fakra, S. C.; Majestic, B. J., Iron Speciation in $PM_{2.5}$ From Urban, Agriculture, and Mixed Environments in Colorado, USA. *Earth and Space Science* **2020,** *7* (10), e2020EA001262.
20. Flocke, F.; Pfister, G.; Crawford, J. H.; Pickering, K. E.; Pierce, G.; Bon, D.; Reddy, P., Air Quality in the Northern Colorado Front Range Metro Area: The Front Range Air Pollution and Photochemistry Experiment (FRAPPE). *Journal of Geophysical Research-Atmospheres* **2020,** *125* (2), e2019JD031197.
21. Doran, J. C., The influence of canyon winds on flow fields near Colorado's Front Range. *Journal of Applied Meteorology* **1996,** *35* (4), 587-600.
22. Johnson, R.; Toth, J. In *Topographic effects and weather forecasting in the Colorado PROFS mesonetwork area. Preprints*, Ninth Conf. on Weather Forecasting and Analysis, 1982; 440-444.
23. Laszakovits, J. R.; Berg, S. M.; Anderson, B. G.; O'Brien, J. E.; Wammer, K. H.; Sharpless, C. M., p-Nitroanisole/Pyridine and p-Nitroacetophenone/Pyridine Actinometers Revisited: Quantum Yield in Comparison to Ferrioxalate. *Environmental Science & Technology Letters* **2017,** *4* (1), 11-14.
24. National Center for Atmospheric Research. 2021. Atmospheric chemistry observations and modeling quick TUV calculator. https://www.acom.ucar.edu/Models/TUV/Interactive_TUV/ (accessed 2021.07.28).
25. Leresche, F.; Torres-Ruiz, J. A.; Kurtz, T.; von Gunten, U.; Rosario-Ortiz., F. L., Optical properties and photochemical production of hydroxyl radical and singlet oxygen after ozonation of dissolved organic matter. *Environmental Science: Water Research & Technology* **2021,** *7*, 346.
26. Rosario-Ortiz, F. L.; Canonica, S., Probe Compounds to Assess the Photochemical Activity of Dissolved Organic Matter. *Environmental Science & Technology* **2016,** *50* (23), 12532-12547.
27. Helms, J. R.; Stubbins, A.; Ritchie, J. D.; Minor, E. C.; Kieber, D. J.; Mopper, K., Absorption spectral slopes and slope ratios as indicators of molecular weight, source, and photobleaching of chromophoric dissolved organic matter. *Limnology and Oceanography* **2008,** *53* (3), 955-969.
28. Lee, H. J.; Aiona, P. K.; Laskin, A.; Laskin, J.; Nizkorodov, S. A., Effect of Solar Radiation on the Optical Properties and Molecular Composition of Laboratory Proxies of Atmospheric Brown Carbon. *Environmental Science & Technology* **2014,** *48* (17), 10217-10226.
29. Liu, J. M.; Lin, P.; Laskin, A.; Laskin, J.; Kathmann, S. M.; Wise, M.; Caylor, R.; Imholt, F.; Selimovic, V.; Shilling, J. E., Optical properties and aging of light-absorbing secondary organic aerosol. *Atmospheric Chemistry and Physics* **2016,** *16* (19), 12815-12827.
30. Kieber, R. J.; Willey, J. D.; Whitehead, R. F.; Reid, S. N., Photobleaching of chromophoric dissolved organic matter (CDOM) in rainwater. *Journal of Atmospheric Chemistry* **2007,** *58* (3), 219-235.
31. Aiona, P. K.; Luek, J. L.; Timko, S. A.; Powers, L. C.; Gonsior, M.; Nizkorodov, S. A., Effect of Photolysis on Absorption and Fluorescence Spectra of Light-Absorbing Secondary Organic Aerosols. *ACS Earth and Space Chemistry* **2018,** *2* (3), 235-245.
32. Wong, J. P. S.; Nenes, A.; Weber, R. J., Changes in Light Absorptivity of Molecular Weight Separated Brown Carbon Due to Photolytic Aging. *Environmental Science & Technology* **2017,** *51* (15), 8414-8421.
33. Ray, D.; Singh, S.; Ghosh, S. K.; Raha, S., Dynamic response of light absorption by PM2.5 bound water-soluble organic carbon to heterogeneous oxidation. *Aerosol Science and Technology* **2019,** *53* (12), 1404-1414.
34. Hems, R. F.; Abbatt, J. P. D., Aqueous Phase Photo-oxidation of Brown Carbon Nitrophenols: Reaction Kinetics, Mechanism, and Evolution of Light Absorption. *ACS Earth and Space Chemistry* **2018,** *2* (3), 225-234.
35. Chen, W.; Westerhoff, P.; Leenheer, J. A.; Booksh, K., Fluorescence excitation - Emission matrix regional integration to quantify spectra for dissolved organic matter. *Environmental Science & Technology* **2003,** *37* (24), 5701-5710.
36. Niu, X. Z.; Liu, C.; Gutierrez, L.; Croue, J. P., Photobleaching-induced changes in photosensitizing properties of dissolved organic matter. *Water Research* **2014,** *66*, 140-148.
37. Rosario-Ortiz, F. L.; Korak, J. A., Oversimplification of Dissolved Organic Matter Fluorescence Analysis: Potential Pitfalls of Current Methods. *Environmental Science & Technology* **2017,** *51* (2), 759-761.
38. P. G. Coble; J. Lead; A. Baker; Reynolds, D. M.; Spencer, R. G. M., Aquatic Organic Matter Fluorescence. In *Aquatic Organic Matter Fluorescence*, Cambridge University Press: Cambridge, 2014; 75-122.
39. Albinet, A.; Minero, C.; Vione, D., Photochemical generation of reactive species upon irradiation of rainwater: Negligible photoactivity of dissolved organic matter. *Science of the Total Environment* **2010,** *408* (16), 3367-3373.

40. Zellner, R.; Exner, M.; Herrmann, H., Absolute OH Quantum Yields in the Laser Photolysis of Nitrate, Nitrite and Dissolved H_2O_2 at 308 and 351 nm in the Temperature range 278-353 K. *Journal of Atmospheric Chemistry* **1990,** *10* (4), 411-425.
41. Paulson, S. E.; Gallimore, P. J.; Kuang, X. B. M.; Chen, J. R.; Kalberer, M.; Gonzalez, D. H., A light-driven burst of hydroxyl radicals dominates oxidation chemistry in newly activated cloud droplets. *Science Advances* **2019,** *5* (5), eaav7689.
42. Liao, C. H.; Kang, S. F.; Wu, F. A., Hydroxyl radical scavenging role of chloride and bicarbonate ions in the H_2O_2/UV process. *Chemosphere* **2001,** *44* (5), 1193-1200.
43. Grebel, J. E.; Pignatello, J. J.; Mitch, W. A., Effect of Halide Ions and Carbonates on Organic Contaminant Degradation by Hydroxyl Radical-Based Advanced Oxidation Processes in Saline Waters. *Environmental Science & Technology* **2010,** *44* (17), 6822-6828.
44. Arakaki, T.; Anastasio, C.; Kuroki, Y.; Nakajima, H.; Okada, K.; Kotani, Y.; Handa, D.; Azechi, S.; Kimura, T.; Tsuhako, A.; Miyagi, Y., A General Scavenging Rate Constant for Reaction of Hydroxyl Radical with Organic Carbon in Atmospheric Waters. *Environmental Science & Technology* **2013,** *47* (15), 8196-8203.
45. Buxton, G. V.; Greenstock, C. L.; Helman, W. P.; Ross, A. B., Critical-Review of Rate Constants for Reactions of Hydrated Electrons, Hydrogen-Atoms and Hydroxyl Radicals ($^{\bullet}OH/^{\bullet}O^{-}$) in Aqueous-Solution. *Journal of Physical and Chemical Reference Data* **1988,** *17* (2), 513-886.
46. Anastasio, C.; McGregor, K. G., Chemistry of fog waters in California's Central Valley: 1. In situ photoformation of hydroxyl radical and singlet molecular oxygen. *Atmospheric Environment* **2001,** *35* (6), 1079-1089.
47. Li, M.; Bao, F. X.; Zhang, Y.; Sheng, H.; Chen, C. C.; Zhao, J. C., Photochemical Aging of Soot in the Aqueous Phase: Release of Dissolved Black Carbon and the Formation of O-1(2). *Environmental Science & Technology* **2019,** *53* (21), 12311-12319.
48. Kaur, R.; Labins, J. R.; Helbock, S. S.; Jiang, W. Q.; Bein, K. J.; Zhang, Q.; Anastasio, C., Photooxidants from brown carbon and other chromophores in illuminated particle extracts. *Atmospheric Chemistry and Physics* **2019,** *19* (9), 6579-6594.
49. Vione, D.; Maurino, V.; Minero, C.; Duncianu, M.; Olariu, R. I.; Arsene, C.; Sarakha, M.; Mailhot, G., Assessing the transformation kinetics of 2-and 4-nitrophenol in the atmospheric aqueous phase. Implications for the distribution of both nitroisomers in the atmosphere. *Atmospheric Environment* **2009,** *43* (14), 2321-2327.
50. Canonica, S.; Jans, U.; Stemmler, K.; Hoigné, J., Transformation kinetics of phenols in water: photosensitization by dissolved natural organic material and aromatic ketones. *Environmental Science & Technology* **1995,** *29* (7), 1822-1831.
51. Boreen, A. L.; Edhlund, B. L.; Cotner, J. B.; McNeill, K., Indirect photodegradation of dissolved free amino acids: The contribution of singlet oxygen and the differential reactivity of DOM from various sources. *Environmental Science & Technology* **2008,** *42* (15), 5492-5498.
52. Apell, J.; McNeill, K., Updated and validated solar irradiance reference spectra for estimating environmental photodegradation rates. *Environmental Science-Processes & Impacts* **2019,** *21* (3), 427-437.
53. O'Dell, K.; Hornbrook, R. S.; Permar, W.; Levin, E. J. T.; Garofalo, L. A.; Apel, E. C.; Blake, N. J.; Jarnot, A.; Pothier, M. A.; Farmer, D. K.; Hu, L.; Campos, T.; Ford, B.; Pierce, J. R.; Fischer, E. V., Hazardous Air Pollutants in Fresh and Aged Western US Wildfire Smoke and Implications for Long-Term Exposure. *Environmental Science & Technology* **2020,** *54* (19), 11838-11847.
54. Zeng, T.; Arnold, W. A., Pesticide photolysis in prairie potholes: probing photosensitized processes. *Environmental Science & Technology* **2013,** *47* (13), 6735-6745.